

GSA Data Repository 2018030

Precise age of *Bangiomorpha pubescens* dates the origin of eukaryotic photosynthesis

Gibson et al.

SUPPLEMENTAL METHODS

Stratigraphy and Sampling

Shale samples were collected from outcrops that lack evidence for secondary mineralization from hydrothermal activity and weathered regions that may have experienced alteration were also avoided. Sample sets comprise several 100–200 g samples excavated 10–30 cm from the outcrop surface to target fresh material. Samples were collected along strike from a narrow stratigraphic range (<10 cm), as well as from a vertical profile (up to 5 m). The most organic-rich and least visibly-weathered samples were then chosen for digestion and isotopic analysis.

Arctic Bay Formation samples are from Shale Valley (N 72° 45' 04.8" W 83° 50' 39.2"), ca. 180 m above the base of section T1413 (Arctic Bay-Adams Sound formations contact not exposed in this locale) and ca. 170 m below the base of the Ikpiarjuk Formation (Angmaat Formation equivalent; Fig. 1). Victor Bay Formation samples are from sections G1431 at Angmaat Mountain (N 72° 09' 25.9" W 79° 02' 05.5") and MB1501 at Pingo Valley (N 72° 53' 48.3" W 81° 24' 45.02"). Both Victor Bay Formation sample sets are from within the same maximum flooding interval indicated by the finest-grained and most organic-rich horizon ca. 25 m above the contact with the Angmaat Formation.

Re-Os Geochronology Methods

Least-weathered samples from each sample set were selected and trimmed with a diamond-tipped lapidary saw blade to remove any weathered surfaces, then polished with a diamond pad to remove any metal contamination. After samples were dried at room temperature, 30–50 g aliquots were crushed to a fine powder (ca. 30 μm) using a SPEX #8506 zirconia ceramic puck and grinding container in a SPEX 8500 shatterbox to homogenize each sample (Kendall et al., 2009a). Analyses of Re and Os isotopic abundances and compositions were performed at the University of Alberta's Re-Os Crustal Geochronology Laboratory in the Department of Earth and Atmospheric Sciences following methodologies developed by Creaser et al. (2002), Selby and (2003), Kendall et al. (2004), and Cumming et al. (2013).

Between 0.2 and 0.5 g of each sample was digested and equilibrated with 8 ml of Cr^{VI} - H_2SO_4 along with a known quantity of mixed $^{185}\text{Re} + ^{190}\text{Os}$ tracer solution (spike) in Carius tubes at 220 °C for 48 hrs. Digestion with Cr^{VI} - H_2SO_4 is known to preferentially liberate hydrogenous rather than detrital Re and Os in shale samples, resulting in more accurate and precise isochrons (Selby and Creaser, 2003; Kendall et al., 2004; Rooney et al., 2011). Osmium was isolated and purified by CHCl_3 solvent extraction and micro-distillation using HBr , and Re was purified using $(\text{CH}_3)_2\text{CO}$ solvent extraction and anion chromatography following protocols outlined by Selby and Creaser (2003) and Cumming et al. (2013). These Re and Os fractions were then loaded onto Ni and Pt filaments, respectively (Selby and Creaser, 2003; Selby et al., 2007), for analysis with a ThermoScientific TRITON instrument using negative thermal ionization mass spectrometry (NTIMS; Creaser et al., 1991). Re was analyzed via static Faraday collection and Os utilizing ion-counting with a secondary electron multiplier in peak-hopping mode.

Isochron ages were regressed using the Re and Os isotopic measurements, calculated 2σ

uncertainties for $^{187}\text{Re}/^{188}\text{Os}$ and $^{187}\text{Os}/^{188}\text{Os}$, and the associated error correlation function (ρ) using Isoplot V. 4.15 (Ludwig, 1980; Ludwig, 2011) with a ^{187}Re decay constant (λ) of $1.666 \times 10^{-11} \text{year}^{-1}$ (Table DR1; Smoliar et al., 1996). A Re standard solution of normal isotopic composition was repeatedly analyzed to monitor long-term mass spectrometry reproducibility, using analysis amounts typical for shale samples (1–4 ng). For this solution, an average value for $^{185}\text{Re}/^{187}\text{Re}$ of 0.5973 ± 0.0007 ($n = 52$; 1σ) was obtained over the period of analysis, which overlaps the value of 0.5974 (Gramlich et al., 1973). A Johnson–Matthey Os solution is used as an in-house standard for Os, which yielded an average $^{187}\text{Os}/^{188}\text{Os}$ ratio of 0.10683 ± 0.00010 ($n = 186$; 1σ) by pulse-counting SEM measurement over the period of analysis, which is identical to values reported elsewhere (Li et al., 2010).

TABLE DR1. Re AND Os ABUNDANCES AND ISOTOPIC COMPOSITIONS

Sample	Formation	Re (ppb)	$\pm 2s$	Os (ppt)	$\pm 2s$	$^{187}\text{Re}/^{188}\text{Os}$	$\pm 2s$	$^{187}\text{Os}/^{188}\text{Os}$	$\pm 2s$	ρ^*	Os_i^\dagger
T1413-181.1 [§]	Arctic Bay	67.31	0.25	1247.38	8.16	757.68	3.48	14.80	0.06	0.54	1.42
T1413-181.8 [§]	Arctic Bay	21.62	0.08	488.94	3.55	490.77	2.97	10.12	0.05	0.73	1.45
T1413-182.0 [§]	Arctic Bay	22.10	0.09	524.52	4.69	445.38	2.98	9.28	0.07	0.62	1.41
T1413-182.6 [§]	Arctic Bay	48.49	0.18	1082.97	7.36	501.16	2.37	10.27	0.05	0.48	1.41
T1413-184.0 [§]	Arctic Bay	16.76	0.07	404.74	3.11	432.12	2.94	9.07	0.06	0.76	1.43
T1413-185.0	Arctic Bay	50.76	0.19	1145.79	8.71	485.80	2.41	9.91	0.05	0.48	1.33
G1431-26.0b [§]	Victor Bay	0.76	0.01	33.38	0.49	166.36	4.32	4.15	0.10	0.66	1.22
G1431-26.0c [§]	Victor Bay	0.72	0.01	24.25	0.39	246.74	7.93	5.61	0.16	0.84	1.27
G1431-28.1 [§]	Victor Bay	0.94	0.01	32.57	0.48	236.08	5.78	5.46	0.12	0.79	1.31
G1431-28.2	Victor Bay	0.94	0.01	32.79	0.43	229.48	5.36	5.21	0.10	0.83	1.18
MB1501-51.6a [§]	Victor Bay	16.73	0.04	406.59	3.41	416.96	2.52	8.58	0.06	0.75	1.24
MB1501-51.6b [§]	Victor Bay	15.52	0.04	384.67	4.13	403.94	3.25	8.39	0.09	0.69	1.28
MB1501-51.7 [§]	Victor Bay	7.04	0.02	187.46	1.58	355.79	2.82	7.54	0.06	0.86	1.28
MB1501-51.9	Victor Bay	12.89	0.03	316.92	2.33	404.81	2.12	8.29	0.05	0.78	1.17

Note: Total procedural blanks analyzed during this study were 11 ± 3 pg Re and 0.25 ± 0.3 pg Os and $^{187}\text{Os}/^{188}\text{Os}$ of 1.3 ± 0.8 ($1\sigma, n=5$).

* ρ = associated error correlation (Ludwig, 1980).

$\dagger \text{Os}_i$ = Initial $^{187}\text{Os}/^{188}\text{Os}$ isotope composition calculated from $\lambda^{187}\text{Re}$ and isochron ages that utilize all samples (1051 Ma for Arctic Bay samples and 1047 Ma for Victor Bay formations samples; Figure DR4).

[§]Samples included in the isochrons that utilized a limited stratigraphic range (Fig. 2).

Cross-Calibrated Molecular Clock (BEAST2) Methods

In lieu of a complete fossil record, molecular clock analyses may be improved by increasing the amount of age data they incorporate. Cross-calibrated analyses leverage relative dating information using gene duplication events to increase the accuracy of divergence time estimates (Shih and Matzke, 2013). Molecular clock analyses were run on a concatenated dataset of proteins: AtpA, AtpB, AtpE, AtpF, AtpH, AtpI, Rpl2, Rpl16, Rps3, Rps12, and Eftu, as well as 16S rDNA. To generate the dataset, sequences were aligned using MAFFT (Kato et al., 2005), then partitioned into the concatenated protein sequences and 16S nucleotide sequences. The base set of age calibrations implemented are primarily from on the fossil records of plants and algae and the molecular clock analyses of Smith et al. (2010). A summary of the various constraints used can be found in Table DR2. A uniform prior of 2.4–3.8 billion years ago (Ga) was used as a constraint for the last common ancestor. The only constraint that differed between the three analyses was the prior set on the green-red divergence, representing the oldest possible node for which *Bangiomorpha pubescens* can provide a direct constraint based on its position either derived within the Bangiales or perhaps as a stem-group red alga (e.g., Butterfield, 2000; Yang et al., 2016). In these analyses (Table 1), three constraints were tested to compare their effect on different interpretations of plastid endosymbiosis: 1) no prior (Run T07; Fig. DR1), 2) a prior based on the previously reported age for *Bangiomorpha pubescens* of 1.198 Ga (Run T08; Fig. DR2; Butterfield, 2000), and 3) a prior based on our geochronology data of 1.045 Ga (Run T09; Fig. DR3). As previously described (Shih et al., 2017), molecular clock analyses were estimated with the program BEAST2 (Drummond and Rambaut, 2007) using the CIPRES Science Gateway server (Miller et al., 2010). The CpREV model and the GTR + G model were used as the substitution model for the protein and nucleotide datasets, respectively. A lognormal

relaxed molecular clock model was implemented. For all analyses, three separate MCMC chains for 40–50 million generations were generated, sampling every 10,000 generations. The initial 20 million generations were discarded as burn-in, and maximum clade credibility trees were generated using TreeAnnotator v1.7.5. The analyses and dates of interest are summarized in the main text and Table 1.

TABLE DR2. SUMMARY OF CALIBRATION CONSTRAINTS USED IN THIS STUDY.

Divergence event	Type of Distribution	Age Constraint (Ga)
Angiospermae	Normal	0.217 ± 0.040 (1σ)
Land Plants	Normal	0.477 ± 0.070 (1σ)
<i>Bangiomorpha pubescens</i>	Uniform	1.174–1.222
“Rise of Oxygen”	Uniform	2.400–3.000
Last Common Ancestor	Uniform	2.400–3.800

Note: Angiospermae and land plant age constraints from Smith et al. (2010).

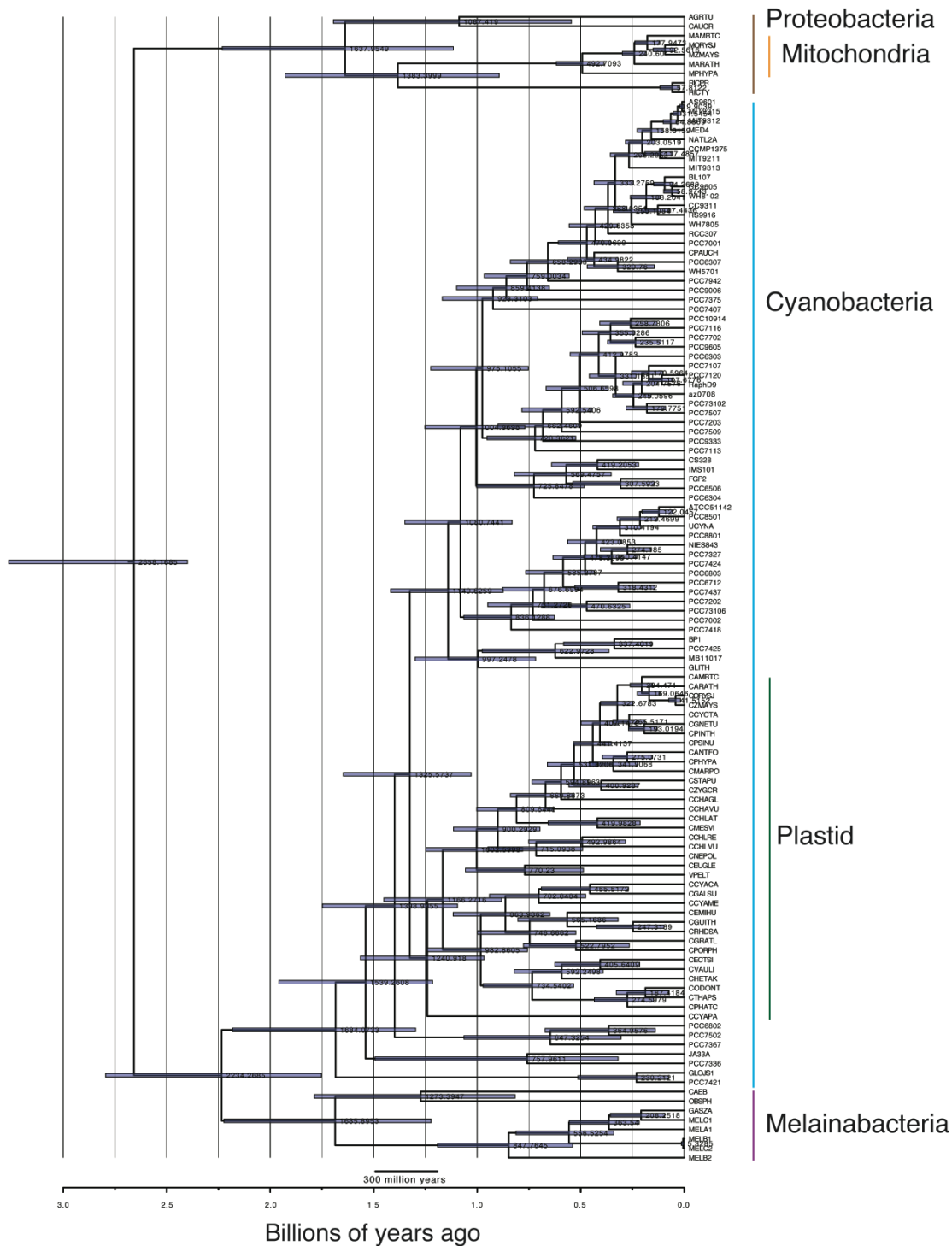


Figure DR1. Divergence time estimates from T07 cross-calibrated BEAST2 run. All land plant constraints were used; however, no *Bangiomorpha pubescens* constraint was utilized. Abbreviations are summarized in Table DR3.

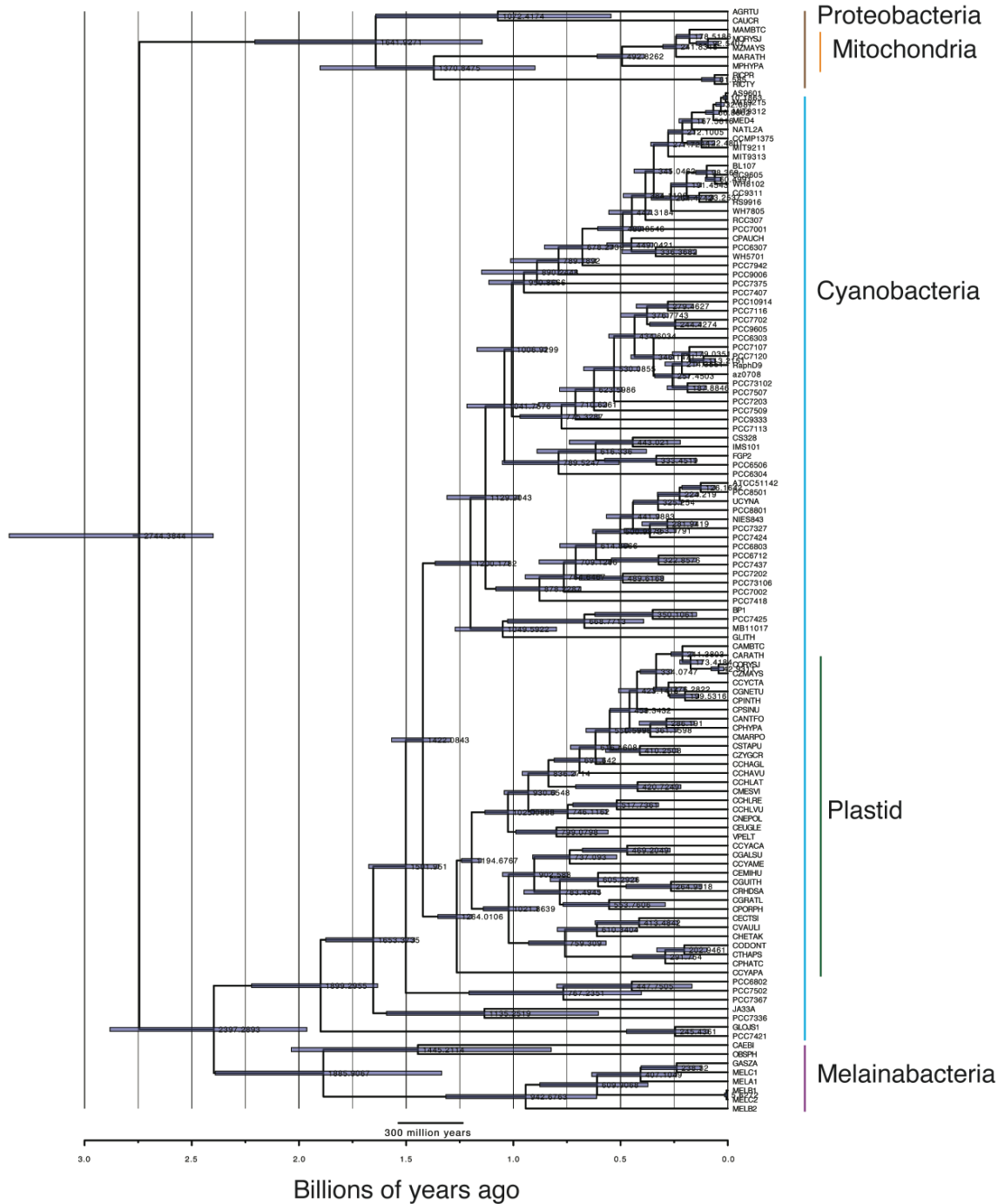


Figure DR2. Divergence time estimates from T08 cross-calibrated BEAST2 run. All land plant constraints were used. *Bangiomorpha pubescens* was constrained to the green-red divergence using the older and previously inferred age of 1.2 Ga. Abbreviations are summarized in Table DR3.

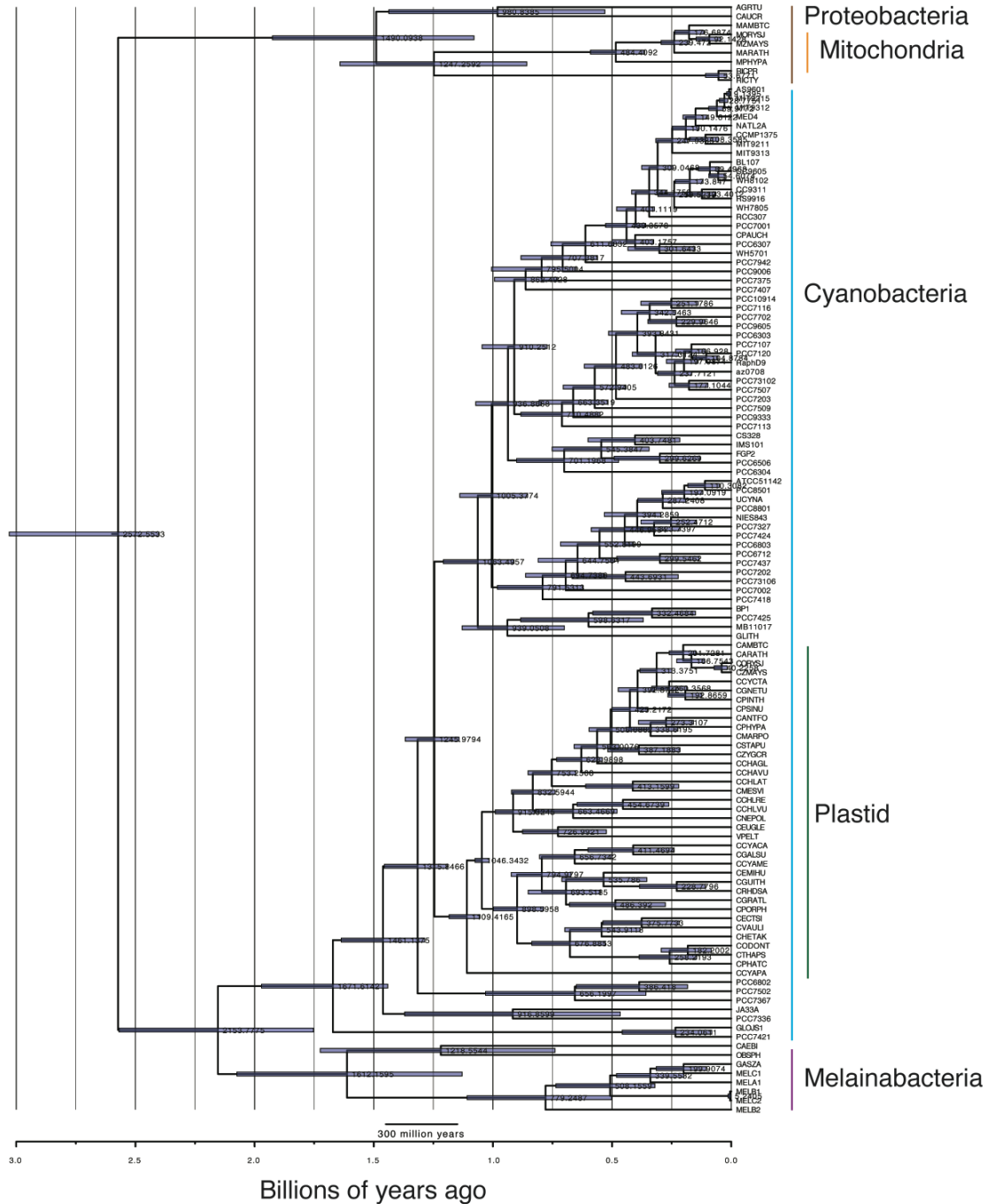


Figure DR3. Divergence time estimates from T09 cross-calibrated BEAST2 run. All land plant constraints were used. *Bangiomorpha pubescens* was constrained to the green-red divergence using the younger, revised age of 1.045 Ga. Abbreviations are summarized in Table DR3.

TABLE DR3. ABBREVIATIONS FOR SPECIES NAMES USED IN FIGURES DR1-3.

Species Name	Clade	Abbreviation
<i>Gloeobacter violaceus</i> PCC 7421	Cyanobacteria	PCC7421
<i>Gloeobacter kilaueensis</i> JS1	Cyanobacteria	GLOJS1
<i>Synechococcus</i> sp. PCC 7336	Cyanobacteria	PCC7336
<i>Synechococcus</i> sp. JA-3-3Ab	Cyanobacteria	JA33A
<i>Pseudanabaena</i> sp. PCC 7367	Cyanobacteria	PCC7367
<i>Pseudanabaena</i> sp. PCC 6802	Cyanobacteria	PCC6802
<i>Synechococcus</i> sp. PCC 7502	Cyanobacteria	PCC7502
<i>Acaryochloris marina</i> MBIC11017	Cyanobacteria	MB11017
<i>Cyanothece</i> sp. PCC 7425	Cyanobacteria	PCC7425
<i>Thermosynechococcus elongatus</i> BP-1	Cyanobacteria	BP1
<i>Geitlerinema</i> sp. PCC 7407	Cyanobacteria	PCC7407
<i>Leptolyngbya</i> sp. PCC 7375	Cyanobacteria	PCC7375
<i>Prochlorothrix hollandica</i> PCC 9006	Cyanobacteria	PCC9006
<i>Synechococcus elongatus</i> PCC 7942	Cyanobacteria	PCC7942
<i>Cyanobium</i> sp. PCC 7001	Cyanobacteria	PCC7001
<i>Cyanobium gracile</i> PCC 6307	Cyanobacteria	PCC6307
<i>Synechococcus</i> sp. WH 5701	Cyanobacteria	WH5701
<i>Synechococcus</i> sp. RS 9916	Cyanobacteria	RS9916
<i>Synechococcus</i> sp. CC 9311	Cyanobacteria	CC9311
<i>Synechococcus</i> sp. WH 7805	Cyanobacteria	WH7805
<i>Synechococcus</i> sp. BL 107	Cyanobacteria	BL107
<i>Synechococcus</i> sp. CC 9605	Cyanobacteria	CC9605
<i>Synechococcus</i> sp. WH 8102	Cyanobacteria	WH8102
<i>Prochlorococcus marinus</i> MIT 9313	Cyanobacteria	MIT9313
<i>Prochlorococcus marinus</i> , subsp. <i>marinus</i> CCMP 1375	Cyanobacteria	CCMP1375
<i>Prochlorococcus marinus</i> MIT 9211	Cyanobacteria	MIT9211
<i>Prochlorococcus marinus</i> MIT 9312	Cyanobacteria	MIT9312
<i>Prochlorococcus marinus</i> MIT 9215	Cyanobacteria	MIT9215
<i>Prochlorococcus marinus</i> AS 9601	Cyanobacteria	AS9601
<i>Prochlorococcus marinus</i> , subsp. <i>pastoris</i> CCMP 1986	Cyanobacteria	MED4
<i>Prochlorococcus marinus</i> NATL 2A	Cyanobacteria	NATL2A
<i>Synechococcus</i> sp. RCC307	Cyanobacteria	RCC307
<i>Crinalium epipsammum</i> PCC 9333	Cyanobacteria	PCC9333
<i>Microcoleus</i> sp. PCC 7113	Cyanobacteria	PCC7113
<i>Chroococciopsis</i> sp. PCC 6712	Cyanobacteria	PCC6712
<i>Stanieria cyanosphaera</i> PCC 7437	Cyanobacteria	PCC7437
<i>Cyanobacterium stanieri</i> PCC 7202	Cyanobacteria	PCC7202
<i>Synechococcus</i> sp. PCC 7002	Cyanobacteria	PCC7002
<i>Gloeocapsa</i> sp. PCC 73106	Cyanobacteria	PCC73106
<i>Cyanothece</i> sp. PCC 7424	Cyanobacteria	PCC7424
<i>Microcystis aeruginosa</i> NIES-843	Cyanobacteria	NIES843
<i>Pleurocapsa</i> sp. PCC 7327	Cyanobacteria	PCC7327
<i>Synechocystis</i> sp. PCC 6803	Cyanobacteria	PCC6803
<i>Cyanothece</i> sp. PCC 8801	Cyanobacteria	PCC8801
<i>Crocospaera watsonii</i> WH 8501	Cyanobacteria	PCC8501
<i>Cyanothece</i> sp. ATCC 51142	Cyanobacteria	ATCC51142
Unidentified cyanobacterium UCYN-A	Cyanobacteria	UCYNA
<i>Halothece</i> sp. PCC 7418	Cyanobacteria	PCC7418
<i>Chroococciopsis thermalis</i> PCC 7203	Cyanobacteria	PCC7203
<i>Synechocystis</i> sp. PCC 7509	Cyanobacteria	PCC7509
<i>Rivularia</i> sp. PCC 7116	Cyanobacteria	PCC7116
<i>Nostoc punctiforme</i> PCC 73102	Cyanobacteria	PCC73102
<i>Calothrix</i> sp. PCC 7507	Cyanobacteria	PCC7507
<i>Nostoc azollae</i> 0708	Cyanobacteria	az0708
<i>Raphidiopsis brookii</i> D9	Cyanobacteria	RaphD9
<i>Nostoc</i> sp. PCC 7107	Cyanobacteria	PCC7107
<i>Nostoc</i> sp. PCC 7120	Cyanobacteria	PCC7120
<i>Calothrix</i> sp. PCC 6303	Cyanobacteria	PCC6303
<i>Mastigocladopsis repens</i> PCC 10914	Cyanobacteria	PCC10914
unidentified cyanobacterium PCC 7702	Cyanobacteria	PCC7702

TABLE DR3 continued. ABBREVIATIONS FOR SPECIES NAMES USED IN FIGURES DR1-3.

Species Name	Clade	Abbreviation
<i>Fischerella</i> sp. PCC 9605	Cyanobacteria	PCC9605
<i>Oscillatoria acuminata</i> PCC 6304	Cyanobacteria	PCC6304
<i>Oscillatoria</i> sp. PCC 6506	Cyanobacteria	PCC6506
<i>Microcoleus vaginatus</i> FGP-2	Cyanobacteria	FGP2
<i>Arthrospira maxima</i> CS-328	Cyanobacteria	CS328
<i>Trichodesmium erythraeum</i> IMS 101	Cyanobacteria	IMS101
<i>Gloeomargarita lithophora</i>	Cyanobacteria	GLITH
MEL.A1	Melainabacteria	MELA1
MEL.B1	Melainabacteria	MELB1
MEL.B2	Melainabacteria	MELB2
MEL.C1	Melainabacteria	MELC1
MEL.C2	Melainabacteria	MELC2
<i>Rickettsia prowazekii</i> strain, Madrid E	α -proteobacteria	RICPR
<i>Rickettsia typhi</i> strain ATCC VR-144	α -proteobacteria	ATPA_RICTY
<i>Caulobacter crescentus</i> strain ATCC 19089	α -proteobacteria	ATPA_CAUCR
<i>Agrobacterium tumefaciens</i> strain C58	α -proteobacteria	ATPA_AGRTU
<i>Arabidopsis thaliana</i>	Plastid	ARATH
<i>Oryza sativa</i> subsp. Japonica	Plastid	ORYSJ
<i>Zea mays</i>	Plastid	ZMAYS
<i>Amborella trichopoda</i>	Plastid	AMBTC
<i>Pinus thunbergii</i>	Plastid	PINTH
<i>Cycas taitungensis</i>	Plastid	CYCTA
<i>Gnetum parvifolium</i>	Plastid	GNETU
<i>Psilotum nudum</i>	Plastid	PSINU
<i>Anthoceros formosae</i>	Plastid	ANTFO
<i>Marchantia polymorpha</i>	Plastid	MARPO
<i>Physcomitrella patens</i> subsp. patens	Plastid	PHYPA
<i>Zygnema circumcarinatum</i>	Plastid	ZYGCR
<i>Staurastrum punctulatum</i>	Plastid	STAPU
<i>Chaetosphaeridium globosum</i>	Plastid	CHAGL
<i>Chara vulgaris</i>	Plastid	CHAVU
<i>Chlamydomonas reinhardtii</i>	Plastid	CHLRE
<i>Chlorella vulgaris</i>	Plastid	CHLVU
<i>Nephroselmis olivacea</i>	Plastid	NEPOL
<i>Euglena gracilis</i>	Plastid	EUGLE
<i>Mesostigma viride</i>	Plastid	MESVI
<i>Chlorokybus atmophyticus</i>	Plastid	CHLAT
<i>Verdigellas peltata</i>	Plastid	VPELT
<i>Cyanophora paradoxa</i>	Plastid	CYAPA
<i>Cyanidioschyzon merolae</i>	Plastid	CYAME
<i>Cyanidium caldarium</i>	Plastid	CYACA
<i>Gracilaria tenuistipitata</i>	Plastid	GRATL
<i>Porphyridium purpureum</i>	Plastid	PORPH
<i>Galdieria sulphuraria</i>	Plastid	GALSU
<i>Thalassiosira pseudonana</i>	Plastid	THAPS
<i>Ectocarpus siliculosus</i>	Plastid	ECTSI
<i>Phaeodactylum tricornutum</i>	Plastid	PHATC
<i>Guillardia theta</i>	Plastid	GUITH
<i>Rhodomonas salina</i>	Plastid	RHDSA
<i>Vaucheria litorea</i>	Plastid	VAULI
<i>Heterosigma akashiwo</i> NIES-293	Plastid	HETAK
<i>Odontella sinensis</i>	Plastid	ODONT
<i>Emiliania huxleyi</i>	Plastid	EMIHU
<i>Paulinella chromatophora</i>	Plastid	PAUCH
<i>Arabidopsis thaliana</i>	Mitochondria	ARATH
<i>Zea mays</i>	Mitochondria	ZMAYS
<i>Oryza sativa</i>	Mitochondria	ORYSJ
<i>Amborella trichopoda</i>	Mitochondria	AMBTC
<i>Physcomitrella patens</i> subsp. patens	Mitochondria	PHYPA

SUPPLEMENTAL TEXT

Rhenium-Osmium Results

Re and Os data from this study (see Table DR1) are within reported concentrations and isotopic ratios of other black shales and do not display evidence for post-depositional disturbance of the Re-Os system. Regression of Arctic Bay Formation samples excluding T1413-181.1 yields a nearly identical age of 1.054 ± 0.041 Ga and confirms that this sample does not disproportionately affect the isochron by “anchoring” its slope. Victor Bay Formation samples are from two correlative stratigraphic sections (G1431 and MB1501). Regression of G1431 Victor Bay Formation samples yield an imprecise Model 3 age of 1.077 ± 0.28 Ga due to an insufficient spread in initial $^{187}\text{Re}/^{188}\text{Os}$ and too much variation in initial $^{187}\text{Os}/^{188}\text{Os}$ values (see Table DR1) necessary to develop a precise isochron (Selby and Creaser, 2005; Kendall et al., 2009a). Therefore, samples from section MB1501 of the same maximum flooding interval in the lower Victor Bay Formation were also incorporated. Regression of MB1501 samples yielded an imprecise, but indistinguishable to G1431 (within uncertainty), Model 3 age of 0.995 ± 0.320 Ga. A sharp transgressive surface directly above the basin-wide Angmaat-Victor Bay unconformity marks a regional flooding event in the Milne Inlet Graben, and offers an unequivocally synchronous datum (Sherman et al., 2001). Sample set G1431 was collected from 26–28.1 m above this unconformity, and sample set MB1501 is from a slightly deeper-water, but time-correlative horizon 21.3–21.6 m above this unconformity. Robust stratigraphic evidence for depositional synchronicity and the similarity of their model ages enable regression of these samples as a combined data set to produce a significantly more precise age (Fig. DR4; Geboy et al., 2013). Combining these data sets is further supported by the relative precision and lower variance in the composite isochron, as well as its agreement with the Re-Os age for the Arctic

Bay Formation reported herein (Fig. 2).

Initial $^{187}\text{Os}/^{188}\text{Os}$ values for all Arctic Bay and Victor Bay samples range from 1.17–1.45 (average modern continental runoff $^{187}\text{Os}/^{188}\text{Os} = 1.5$; Levasseur et al., 1999), consistent with a highly radiogenic Os flux dominated by evolved, continentally derived sediment and waters (Xu et al., 2009; Cumming et al., 2012; Cumming et al., 2013; Rooney et al., 2014). These data demonstrate that the Borden Basin had minimal communication with the global ocean during deposition of the sampled black shale units from the middle Arctic Bay (Turner and Kamber, 2012; Hahn et al., 2015) and lower Victor Bay formations and was strongly influenced chemically by runoff from the surrounding highly-evolved Archean to Paleoproterozoic orthogneiss and metasedimentary successions of the Rae Province (Crocker et al., 1993). However, abundant sulfate evaporite deposits, marine C, S, and Sr isotopic signatures, and evidence for tidal influence indicate that the Borden Basin was connected to a large ocean basin during deposition of the Angmaat Formation and other intervals of carbonate deposition (i.e. upper Victor Bay and Athole Point formations; Kah et al., 1999; Kah et al., 2001). Together these data demonstrate that the Borden Basin was periodically restricted from the open ocean and that the degree of restriction influenced sedimentation patterns, perhaps due to changes in the geochemical stratification of its basin waters. These interpretations may help characterize the environment in which *Bangiomorpha pubescens* evolved.

Precise Re-Os isochrons require samples of the same (or similar) age and with similar initial $^{187}\text{Os}/^{188}\text{Os}$ (Cohen et al., 1999; Creaser et al., 2002; Cohen, 2004). Sediment in restricted basins are known to exhibit highly variable $^{187}\text{Os}/^{188}\text{Os}$ as they are sensitive to short-term variability in weathering sources and runoff (McArthur et al., 2008; Cumming et al., 2012; Cumming et al., 2013; Tripathy et al., 2015). Therefore, on the condition that a sufficient spread

in $^{187}\text{Re}/^{188}\text{Os}$ is maintained, utilizing samples from a reduced stratigraphic interval, especially from restricted basins, can minimize age uncertainty by limiting the depositional timescale over which samples were deposited and thus stratigraphic variation in initial $^{187}\text{Os}/^{188}\text{Os}$ (Os_i ; Xu et al., 2009; Cumming et al., 2012; Xu et al., 2014).

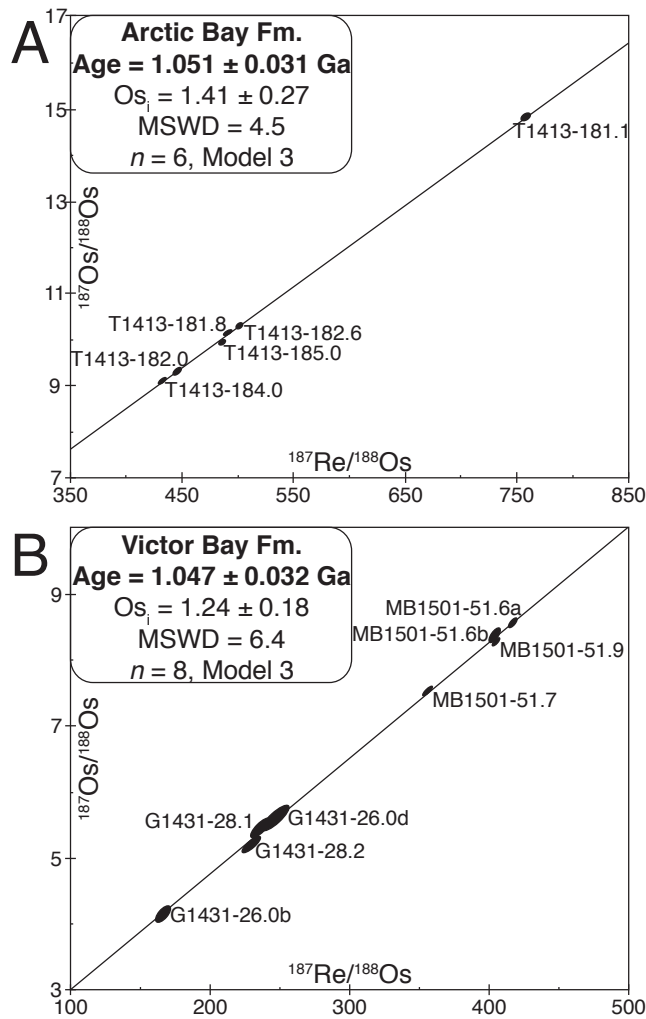


Figure DR4. Re-Os geochronological data and isochron diagrams for all Arctic Bay (A) and Victor Bay (B) formations samples. Mean square of weighted deviation (MSWD) values greater than unity (i.e., 1) indicate that geological factors rather than analytical error are responsible for scatter about the isochron (Mahon, 1996). Data-point error ellipses represent 2σ uncertainty. Elemental abundances and isotopic compositions are presented in Table DR1.

Previous Geochronology from the Bylot Supergroup

Pyrite Re-Os geochronology from the carbonate-hosted Nanisivik Pb-Zn deposit (Angmaat Formation equivalent; see Fig. 1) suggest approximately syn-depositional mineralization ca. 1.1 billion years ago (Ga), though the data span 1.151-1.013 Ga (Hnatyshin et al., 2016), which is broadly consistent with depositional ages presented from this study. Turner and Kamber (2012) conducted whole-rock U-Th-Pb analyses of Arctic Bay Formation black shales and calculated an age of 1.092 ± 0.059 Ga from the weighted mean of a ^{206}Pb - ^{207}Pb isochron and ^{238}U - ^{206}Pb and ^{232}Th - ^{208}Pb errorchrons; however, a total of nine outlying samples were excluded in these calculations and stratigraphic heights are not reported.

Unpublished whole-rock, carbonate Pb-Pb geochronology of Angmaat Formation samples were reported to produce an age of 1.199 ± 0.024 Ga, and combined data from Angmaat, Victor Bay, and Athole Point formations samples an age of 1.204 ± 0.022 Ga (Kah et al., 2001). While these dates were often cited as the age of *Bangiomorpha pubescens* (ca. 1.2 Ga), they are older than and therefore incompatible with the calculated age of the underlying Arctic Bay Formation from Turner and Kamber (2012). Furthermore, Pb-Pb carbonate ages can overestimate depositional ages due to incorporation of basement-derived Pb during diagenesis (i.e., dolomitization), meteoric alteration, and metamorphism (e.g., Babinski et al., 2007). These incongruent ages highlight obstacles associated with the application of whole-rock U-Th-Pb and Pb-Pb geochronology to typical Precambrian samples. The utility of the black shale Re-Os geochronometer for yielding precise and accurate ages of Precambrian sedimentary successions, on the other hand, is corroborated by numerous recent studies (e.g., Selby and Creaser, 2003; Kendall et al., 2009b; Cumming et al., 2013; van Acken et al., 2013; Rooney et al., 2014; Rooney et al., 2015).

Age of the Chitrakoot Taxa

The Vindhyan Supergroup in central India has long been the center of debate regarding fossil discoveries and their ages (see Ray, 2006 for overview). This up-to 4-km-thick sedimentary succession primarily outcrops in the Son Valley and Rajasthan. The lower Vindhyan Semri Group has largely been studied in the Son Valley region where multiple interbedded volcanic tuffs offer robust U-Pb zircon depositional age constraints of ca. 1.6 Ga (Rasmussen et al., 2002; Ray et al., 2002; Bengtson et al., 2009). These ages are broadly consistent with the occurrence of microfossils such as *Grypania* (Kumar, 1995) which occur globally in strata of similar ages (Adams et al., 2017).

The Chitrakoot Formation occurs as a stratigraphic outlier in the Jankikund-Chitrakoot region to the north of the Son Valley, and is interpreted to record deposition within an isolated sub-basin that was disconnected from the main Vindhyan basin (Bose et al., 2015); however, discontinuous lateral exposure renders robust correlations, even within the Chitrakoot region, tenuous. The Chitrakoot Formation has been dated using whole-rock geochronological techniques, with whole-rock Rb-Sr ages from lower glauconitic facies spanning ca. 1.5–1.4 Ga (Kumar et al., 2001), and a whole-rock Pb-Pb age of 1.65 ± 0.089 Ga from the uppermost phosphatic Tirohan Dolomite (Bengtson et al., 2009). While these dates broadly support correlation between the Tirohan Dolomite of the Chitrakoot Formation and the Rohtas Limestone of the Semri Group (Bengtson et al., 2017), robust stratigraphic correlations between the Chitrakoot outlier and principal Vindhyan sections in the Son Valley are complicated by inconclusive chemostratigraphic signatures (Ray et al., 2003) and significant lithological and thickness differences between these successions (Chakraborty, 2006). Alternately, if the Tirohan Dolomite is equivalent to the next younger unit that directly overlies the Rohtas Limestone, it

would belong to the upper Vindhyan Kaimur Group which could be as young as ca. 1.07 Ga (Gregory et al., 2006)—similar to the age of the Angmaat Formation. Thus, the ca. 1.6 Ga age of the phosphatized fossils from the Tirohan Dolomite is primarily based on the internally inconsistent dates for the Chitrakoot Formation, and so further corroboration of the anomalously old age of these fossils requires the application of reliable, high precision geochronology to the Chitrakoot sections themselves.

Author Contributions T.M.G., P.M.S., W.W.F., R.H.R., T.M.S., and G.P.H. conceived the project. T.M.G., P.M.S., W.W.F., and G.P.H. wrote the manuscript with input from all coauthors. T.M.G., V.M.C., P.W.C., S.W., M.S.W.H. and G.P.H. executed fieldwork and sample collection. T.M.G., V.M.C. and R.A.C. carried out Re-Os measurements and data analysis. P.M.S. executed molecular clock analyses.

REFERENCES CITED:

- Adams, Z.R., Skidmore, M.L., Mogk, D.W., and Butterfield, N.J., 2017, A Laurentian record of the earliest fossil eukaryotes: *Geology*, v. 45, p. 387–390, doi:10.1130/G38749.1.
- Babinski, M., Vieira, L.C., Trindade, R.I.F., 2007, Direct dating of the Sete Lagoas cap carbonate (Bambuí Group, Brazil) and implications for the Neoproterozoic glacial events: *Terra Nova*, v. 19, p. 401–406, doi:10.1111/j.1365-3121.2007.00764.x.
- Bengtson, S., Belivanova, V., Rasmussen, B., and Whitehouse, M., 2009, The controversial “Cambrian” fossils of the Vindhyan are real but more than a billion years older: *Proceedings of the National Academy of Sciences*, v. 106, p. 7729–7734, doi:10.1073/pnas.0812460106.

- Bengtson, S., Sallstedt, T., Belivanova, V., and Whitehouse, M., 2017, Three-dimensional preservation of cellular and subcellular structures suggests 1.6 billion-year-old crown-group red algae: *PLoS Biology*, v. 15, e2000735, doi:10.1371/journal.pbio.2000735.
- Bose, P.K., Sarkar, S., Das, N.G., Banerjee, S., Mandal, A., and Chakraborty, N., 2015, Proterozoic Vindhyan Basin: Configuration and evolution: Bose PK, Sarkar S, Das NG, Banerjee S, Mandal A, Chakraborty N. Proterozoic Vindhyan Basin: configuration and evolution: Geological Society, London, Memoirs, v. 43, p. 85–102, doi:10.1144/M43.6.
- Butterfield, N.J., 2000, *Bangiomorpha pubescens* n. Gen., n. sp.: Implications for the evolution of sex, multicellularity, and the Mesoproterozoic/ Neoproterozoic radiation of eukaryotes: *Paleobiology*: *Paleobiology*, v. 26, p. 386–404, doi:10.1666/0094-8373(2000)026<0386:BPNGNS>2.0.CO;2.
- Chakraborty, C., 2006, Proterozoic intracontinental basin: The Vindhyan example: *Journal of Earth System Science*, v. 115, p. 3–22, doi:10.1007/BF02703022.
- Cohen, A.S., Coe, A.L., Bartlett, J.M., and Hawkesworth, C.J., 1999, Precise Re–Os ages of organic-rich mudrocks and the Os isotope composition of Jurassic seawater: *Earth and Planetary Science Letters*, v. 167, p. 159–173, doi:10.1016/S0012-821X(99)00026-6.
- Cohen, A.S., 2004, The rhenium–osmium isotope system: applications to geochronological and palaeoenvironmental problems: *Journal of the Geological Society of London*, v. 161, p. 729–734, doi:10.1144/0016-764903-084.
- Creaser, R. A., Papanastassiou, D. A., and Wasserburg, G. J., 1991, Negative thermal ion mass spectrometry of osmium, rhenium and iridium: *Geochimica et Cosmochimica Acta*, v. 55, p. 397-401, doi:10.1016/0016-7037(91)90427-7.
- Creaser, R.A., Sannigrahi, P., Chacko, T., and Selby, D., 2002. Further evaluation of the Re–Os

- geochronometer in organic-rich sedimentary rocks: a test of hydrocarbon maturation effects in the Exshaw Formation, Western Canada Sedimentary Basin: *Geochimica et Cosmochimica Acta*, v. 66, p. 3441–3452, doi:10.1016/S0016-7037(02)00939-0.
- Crocker, C.H., Collerson, K.D., Lewry, J.F. and Bickford, M.E., 1992, Sm-Nd, U-Pb and Rb-Sr geochronology and lithostructural relationships in the southwestern Rae province: constraints on crustal assembly in the western Canadian shield: *Precambrian Research*, v. 61, p. 27–50, doi:10.1016/0301-9268(93)90056-8.
- Cumming, V.M., Selby, D., and Lillis, P.G., 2012, Re-Os geochronology of the lacustrine Green River Formation: Insights into direct depositional dating of lacustrine successions, Re-Os systematics, and paleocontinental weathering: *Earth and Planetary Science Letters*, v. 359-360, p. 194–205, doi:10.1016/j.epsl.2012.10.012.
- Cumming, V.M., Poulton, S.W., Rooney, A.D., and Selby, D., 2013, Anoxia in the terrestrial environment during the late Mesoproterozoic: *Geology*, v. 41, p. 583–586, doi:10.1130/G34299.1.
- Drummond, A.J., and Rambaut, A., 2007, BEAST: Bayesian evolutionary analysis by sampling trees: *BMC Evolutionary Biology*, v. 7, p. 214, doi:10.1186/1471-2148-7-214.
- Geboy, N.J., Kaufman, A.J., Walker, R.J., Misi, A., de Oliveira, T.F., Miller, K.E., Azmy, K., Kendall, B., and Poulton, S.W., 2013, Re-Os age constraints and new observations of Proterozoic glacial deposits in the Vazante Group, Brazil: *Precambrian Research*, v. 238, p. 199–213, doi:10.1016/j.precamres.2013.10.010.
- Gramlich, J.W., Murphy, T.J., Garner, E.L., and Shields, W.R., 1973, Absolute isotopic abundance ratio and atomic weight of a reference sample of Rhenium: *Journal of Research of the National Bureau of Standards*, v. 77A, p. 691–698.

- Gregory, L.C., Meert, J.G., Pradhan, V., Pandit, M.K., Tamrat, E., and Malone, S.J., 2006, A paleomagnetic and geochronologic study of the Majhgawan kimberlite, India: Implications for the age of the Upper Vindhyan Supergroup: *Precambrian Research*, v. 149, p. 65–75, doi:10.1016/j.precamres.2006.05.005.
- Hahn, K.E., Turner, E.C., Babechuk, M.G., and Kamber, B.S., 2015, Deep-water seep-related carbonate mounds in a Mesoproterozoic alkaline lake, Borden Basin (Nunavut, Canada): *Precambrian Research*, v. 271, p. 173–197, doi:10.1016/j.precamres.2015.09.025.
- Hnatyshin, D., Kontak, D.J., Turner, E.C., Creaser, R.A., Morden, R., and Stern, R.A., 2016, Geochronologic (Re–Os) and fluid-chemical constraints on the formation of the Mesoproterozoic-hosted Nanisivik Zn–Pb deposit, Nunavut, Canada: Evidence for early diagenetic, low-temperature conditions of formation: *Ore Geology Reviews*, v. 79, p. 189–217, doi:10.1016/j.oregeorev.2016.05.017.
- Kah, L.C., Sherman, A.G., Narbonne, G.M., Knoll, A.H., and Kaufman, A.J., 1999, $\delta^{13}\text{C}$ stratigraphy of the Proterozoic Bylot Supergroup, Baffin Island, Canada: Implications for regional lithostratigraphic correlations: *Canadian Journal of Earth Sciences*, v.36, p. 313–332, doi:10.1139/e98-100.
- Kah, L.C., Lyons, T.W., and Chesley, J.T., 2001, Geochemistry of a 1.2 Ga carbonate-evaporite succession, northern Baffin and Bylot Islands: implications for Mesoproterozoic marine evolution: *Precambrian Research*, v. 111, p. 1–32, doi:10.1016/S0301-9268(01)00161-9.
- Katoh, K., Kuma, K.-i., Toh, H., and Miyata, T., 2005, MAFFT version 5: Improvement in accuracy of multiple sequence alignment: *Nucleic Acids Research*, v. 33, p. 511–518, doi:10.1093/nar/gki198.

- Kendall, B.S., Creaser, R.A., Ross, G.M., and Selby, D., 2004. Constraints on the timing of Marinoan 'Snowball Earth' glaciation by ^{187}Re – ^{187}Os dating of a Neoproterozoic post-glacial black shale in Western Canada: *Earth and Planetary Science Letters*, v. 222, p. 729–740, doi:10.1016/j.epsl.2004.04.004.
- Kendall, B., Creaser, R.A., Gordon, G.W., and Anbar, A.D., 2009a, Re-Os and Mo isotope systematics of black shales from the Middle Proterozoic Velkerri and Wollongorang Formations, McArthur Basin, northern Australia: *Geochimica Cosmochimica Acta*, v. 73, p. 2534–2558, doi:10.1016/j.gca.2009.02.013.
- Kendall, B., Creaser, R.A., and Selby, D., 2009b, ^{187}Re – ^{187}Os geochronology of Precambrian organic-rich sedimentary rocks: *Geological Society of London Special Publications*, v. 326, p. 85–107, doi:10.1144/SP326.5.
- Kumar, S., 1995, Megafossils from the Mesoproterozoic Rohtas Formation (the Vindhyan Supergroup), Katni area, central India: *Precambrian Research*, v. 72, p. 171–184, doi:10.1016/0301-9268(94)00085-6.
- Kumar, A., Gopalan, K., and Rajagopalan, G., 2001, Age of the Lower Vindhyan sediments, Central India: *Current Science–Bangalore*, v. 81, p. 806–809.
- Levasseur, S., Birck, J.L., and Allegre, C.J., 1999, The osmium riverine flux and the oceanic mass balance of osmium: *Earth and Planetary Science Letters*, v. 174, p. 7–23, doi:10.1016/S0012-821X(99)00259-9.
- Li, J., Liang, X.-R., Xu, J.-F., Suzuki, K., and Dong, Y.-H., 2010, Simplified technique for the measurements of Re-Os isotope by multicollector inductively coupled plasma mass

- spectrometry (MC-ICP-MS): *Geochemical Journal*, v. 44, p. p. 73-80, doi:
10.2343/geochemj.1.0044.
- Ludwig, K. R., 1980, Calculation of uncertainties of U-Pb isotope data: *Earth and Planetary Science Letters*, v. 46, p. 212-220, doi:10.1016/0012-821X(80)90007-2.
- Ludwig, K.R., 2011, Isoplot/Ex, Version 4.15: A geochronological toolkit for Microsoft Excel: *Geochronology Center Berkeley*, v. 4, p.1-70.
http://www.bgc.org/isoplot_etc/isoplot.html.
- Mahon, K.I., 1996, The new “York” Regression: Application of an improved statistical method to geochemistry: *International Geology Reviews*, v. 38, p. 293–303,
doi:10.1080/00206819709465336.
- McArthur, J.M., Algeo, T.J., van de Schootbrugge, B., Li, Q., and Howarth, R.J., 2008, Basinal restriction, black shales, Re-Os dating, and the Early Toarcian (Jurassic) oceanic anoxic event: *Paleoceanography*, v. 23, p. p. 1–22, doi:10.1029/2008PA001607.
- Miller, M.A., Pfeiffer, W., and Schwartz, T., 2010, Creating the CIPRES Science Gateway for inference of large phylogenetic trees: In *Gateway Computing Environments Workshop (GCE)*, p. 1–8, doi:10.1109/GCE.2010.5676129.
- Rasmussen, B., Bose, P.K., Sarkar, S., Banerjee, S., Fletcher, I.R., and McNaughton, N.J., 2002, 1.6 Ga U-Pb zircon age for the Chorhat Sandstone, lower Vindhyan, India: Possible implications for the early evolution of animals: *Geology*, v. 30, p. 103–106,
doi:10.1130/0091-7613(2002)030<0103:GUPZAF>2.0.CO;2.
- Ray, J.S., Martin, M.W., Veizer, J., and Bowring, S.A., 2002, U-Pb zircon dating and Sr isotope systematics of the Vindhyan Supergroup, India: *Geology*, v. 30, p. 131–134,
doi:10.1130/0091-7613(2002)030<0131:UPZDAS>2.0.CO;2.

- Ray, J.S., Veizer, J., and Davis, W.J., 2003, C, O, Sr and Pb isotope systematics of carbonate sequences of the Vindhyan Supergroup, India: age, diagenesis, correlations and implications for global events: *Precambrian Research*, v. 121, p. 103–140, doi:10.1016/S0301-9268(02)00223-1.
- Ray, J.S., 2006, Age of the Vindhyan Supergroup: a review of recent findings: *Journal of Earth System Science*, v. 115, p. 149–160, doi:10.1007/BF02703031.
- Rooney, A.D., Chew, D.M., and Selby, D., 2011, Re-Os geochronology of the Neoproterozoic-Cambrian Dalradian Supergroup of Scotland and Ireland: Implications for Neoproterozoic stratigraphy, glaciations, and Re-Os systematics: *Precambrian Research*, v. 185, p. 202–214, doi:10.1016/j.precamres.2011.01.009.
- Rooney, A.D., Macdonald, F.A., Strauss, J.V., Dudas, F.O., Hallman, C., and Selby, D., 2014, Re-Os geochronology and coupled Os-Sr isotope constraints on the Sturtian Snowball Earth: *Proceedings of the National Academy of Sciences*, v. 111, p. 51–56, doi:10.1073/pnas.1317266110.
- Rooney, A.D., Strauss, J.V., Brandon, A.D., and Macdonald, F.A., 2015, A Cryogenian chronology: Two long-lasting synchronous Neoproterozoic glaciations: *Geology*, v. 43, p. 459–462, doi:10.1130/G36511.1.
- Selby, D., and Creaser, R.A., 2003. Re–Os geochronology of organic rich sediments: an evaluation of organic matter analysis methods: *Chemical Geology*, v. 200, p. 225–240, doi:10.1016/S0009-2541(03)00199-2.
- Selby, D., and Creaser, R.A., 2005, Direct radiometric dating of the Devonian-Mississippian time-scale boundary using the Re-Os black shale geochronometer: *Geology* v. 33, p. 545–548, doi:10.1130/G21324.1.

- Selby, D., Creaser, R.A., Stein, H.J., Markey, R.J., and Hannah, J.L., 2007, Assessment of the ^{187}Re decay constant by cross calibration of Re–Os molybdenite and U–Pb zircon chronometers in magmatic ore systems: *Geochimica et Cosmochimica Acta*, v. 71, p. 1999–2013, doi:10.1016/j.gca.2007.01.008.
- Sherman, A.G., Narbonne, G.M., and James, N.P., 2001, Anatomy of a cyclically packaged Mesoproterozoic carbonate ramp in northern Canada: *Sedimentary Geology*, v. 139, p. 171–203, doi:10.1016/S0037-0738(00)00168-8.
- Shih, P.M., and Matzke, N.J., 2013, Primary endosymbiosis events date to the later Proterozoic with cross-calibrated phylogenetic dating of duplicated ATPase proteins: *Proceedings of the National Academy of Sciences*, v. 110, p. 12355–12360, doi:10.1073/pnas.1305813110.
- Shih, P.M., Hemp, J., Ward, L.M., Matzke, N.J., and Fischer, W.W., 2017, Crown group Oxyphotobacteria postdate the rise of oxygen: *Geobiology*, v. 15, p. 19–20, doi:10.1111/gbi.12200.
- Smoliar, M.I., Walker, R.J., and Morgan, J.W., 1996, Re–Os ages of Group IIA, IIIA, IVA and IVB iron meteorites: *Science*, v. 271, p. 1099–1102, doi: 10.1126/science.271.5252.1099.
- Smith, S.A., Beaulieu, J.M., and Donoghue, M.J., 2010, An uncorrelated relaxed-clock analysis suggests an earlier origin for flowering plants: *Proceedings of the National Academy of Sciences*, v. 107, p. 5897–5902, doi:10.1073/pnas.1001225107.
- Tripathy, G.R., and Singh, S.K., 2015, Re–Os depositional age for black shales from the Kaimur Group, Upper Vindhyan, India: *Chemical Geology*, v. 4.13, p. 63–72, doi:10.1016/j.chemgeo.2015.08.011.
- Turner, E.C., and Kamber, B.S., 2012, Arctic Bay Formation, Borden Basin, Nunavut

- (Canada): Basin evolution, black shale, and dissolved metal systematics in the Mesoproterozoic ocean: *Precambrian Research*, v. 208, p. 1–18, doi:10.1016/j.precamres.2012.03.006.
- van Acken, D., Thomson, D., Rainbird, R.H., and Creaser, R.A., 2013, Constraining the depositional history of the Neoproterozoic Shaler Supergroup, Amundsen Basin, NW Canada: Rhenium-osmium dating of black shales from the Wynniatt and Boot Inlet Formations: *Precambrian Research*, v. 236, p. 124–131, doi:10.1016/j.precamres.2013.07.012.
- Xu, G., Hannah, J.L., Stein, H.J., Bingen, B., Yang, B., Zimmerman, A., Weitschat, W., Mork A., and Weiss, H., 2009, Re-Os Geochronology of Arctic black shales to evaluate the Anisian-Ladinian boundary and global faunal correlations: *Earth and Planetary Science Letters*, v. 288, p. 581–587, doi:10.1016/j.epsl.2009.10.022
- Xu, G., Hannah, J.L., Stein, H.J., Mork A., Vigran, J.O., Bingen, B., Schutt, D.L., and Lundschieen, B.A., 2014, Cause of Upper Triassic climate crisis revealed by Re–Os geochemistry of Boreal black shales: *Palaeogeography, Palaeoclimatology, Palaeoecology*, v. 395, p. 222–232, doi:10.1016/j.palaeo.2013.12.027.
- Yang, E.C., Boo, S.M., Battacharya, D., Saunders, G.W., Knoll, A.H., Fredericq, S., Graf, L., and Yoon, H.S., 2016, Divergence time estimates and the evolution of major lineages in the florideophyte red algae: *Nature*, v. 6, p. 21361, doi:10.1038/srep21361.